Available online at www.sciencedirect.com

ScienceDirect

IFAC Papers Online CONFERENCE PAPER ARCHIVE

IFAC PapersOnLine 55-37 (2022) 536–541

On Enhancing the Bandwidth of the Actuator Dynamics in a Multi-rotor Aerial Vehicle

Sesha N. Charla * **Bin Yao** ** **Richard M. Voyles** ***

* *School of Mechanical Engineering, Purdue University, IN 47907 USA (e-mail: scharla@purdue.edu)*
** *School of Mechanical Engineering, Purdue University, IN 47907 USA (e-mail: byao@purdue.edu)*
*** *Polytechnic Institute, Purdue University, IN 47907 USA (e-mail: rvoyles@purdue.edu)*

Abstract: In this work we propose and demonstrate a method for increasing the frequency response bandwidth of actuator dynamics in a multi-rotor vehicle through open-loop compensation. The limitations of such method due to non-linearities in the dynamics are discussed. This method retains the existing electromechanical architecture as no additional sensing is required. The compensator design is based on the identified dynamics considering the non-linear phenomena. This ensures the compensator's performance within the operating range of system. The actuator dynamics are identified experimentally and the effectiveness of the compensation is demonstrated using the same hardware setup.

Keywords: Control Design; Modelling, Identification and Signal Processing; Sensors and Actuators

1. INTRODUCTION

The fully actuated designs of unmanned aerial vehicles (UAVs) have gained a lot of prominence over recent years for aerial manipulation (Ding et al. (2021), Ryll et al. (2017)). Dexterous hexrotor is one such design with applications in physical interactions with structures (Jiang et al. (2017)). A notable design feature includes tilted propellers allowing independent control over the six degrees of freedom in a limited region of the state space. The rotational inertia and mass of the large propeller blades result in actuator dynamics with time-scales comparable to that of the dynamics of the drone effecting the performance in application of precise and controllable forces (Hamandi et al. (2021)). In fact, the survey of Hamandi et al. (2021) noted gaps in the literature coverage regarding theoretical analysis of actuation limits for multi-rotor UAVs. As a possible solution, the present work proposes an open-loop compensator design methodology of enhancing the bandwidth without altering the electromechanical design. The bandwidth of a dynamical system is the frequency range over which the transmission from input to output is effective in bolstering some form of performance. It is a measure of quickness in the response of the system (Townsend and Salisbury (1989)). The present work increases the *open-loop response bandwidth of the actuator dynamics* with PWM signals as input and thrust as output. Consequently, this boosts the closed-loop bandwidth of the multi-rotor vehicle. In the present work, bandwidth is estimated by finding the smallest frequency at which the response magnitude drops by 3 dB from the static value in the frequency response plot (Skogestad and Postlethwaite (2007)).

The motor-propeller dynamics in the context of multi-rotor vehicles are modelled either as input non-linearities or uncertainties (Yacef et al. (2016)), linear dynamics (Pounds et al. (2010)), stationary mappings (Tayebi and McGilvray (2006)) or incorporated into the multi-rotor dynamics (Liang et al. (2021), Wang et al. (2018)). The conditions of validity and model fidelity depends on the frequency range and the nominal conditions. In the present work, the model structure is determined based on the results of non-parametric frequency domain system identification (Ljung et al. (1987)) within the predetermined frequency range. Corresponding parameters are estimated at various nominal inputs with in the operating range of the actuator. This guarantees the performance of the compensator designed across the operating range of inputs and frequencies. A feedback controller using rpm (rotations per minute) of the motor-propeller system as feedback to speed-up (Pounds et al. (2009)) or linearize (Franchi and Mallet (2017)) the dynamics would require additional hardware whose noise characteristics have to be handled separately. Moreover, such a design would have to independently consider the PWM (or voltage) to rpm and rpm to thrust dynamics. The open-loop compensator design approach proposed in the present work does not alter the existing electromechanical design of the actuator.

The paper is organized into five sections. Following introduction, in Section 2 the experimental setup and constraints on input frequency range are presented. The system identification method and the results are discussed in Section 3. In Section 4, the open-loop compensator design is discussed followed by demonstration of its effectiveness

10.1016/j.ifacol.2022.11.238

in increasing the bandwidth. The paper concludes with a few remarks in Section 5.

2. EXPERIMENTAL SETUP

A 1 cm diameter carbon fiber tube, motor mounts and supports cutout off a 1 in thick sheet of plastic are assembled to form the support structure upon which the BLDC motor is mounted (Figure 1). A silicon strain gauge based force sensor, ATI-gamma-FT9809, is mounted on the base of the structure such that the thrust direction of the propeller is aligned with its $X-axis$. The acquisition rate is set to $5\,kHz$ which is found to be greater than the Nyquist frequency for capturing noise and other disturbances. The sensor is interfaced through LabView for data acquisition.

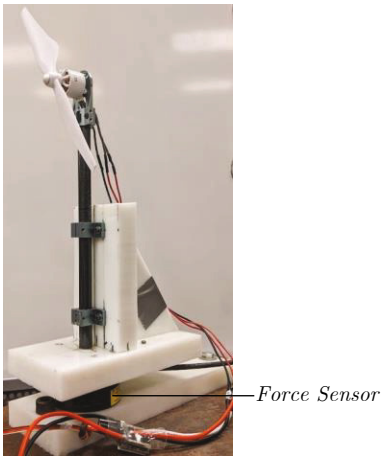

Fig. 1. Experimental setup for system identification

The motor-propeller system whose dynamics are to be identified consists of DJI Phantom T-Motor version-3 of $920\,kv$, DJI-9450 self-tightening composite propeller and an AIR $20\,A$, $600\,Hz$ ESC. The system is controlled using NI-myRio-1900 embedded device which runs a real-time loop at $5\,kHz$. The input to the system is measured in PWM duty cycles as ratio, 0 corresponding to 0 % duty cycle and 1 corresponding to 100 % duty cycle. The output thrust force is measured in Newtons (N). The stationary mapping between the input and output of the system (Figure 2) show that static relationship is non-linear. This confirms variation of static gain of the linearized system with the nominal input.

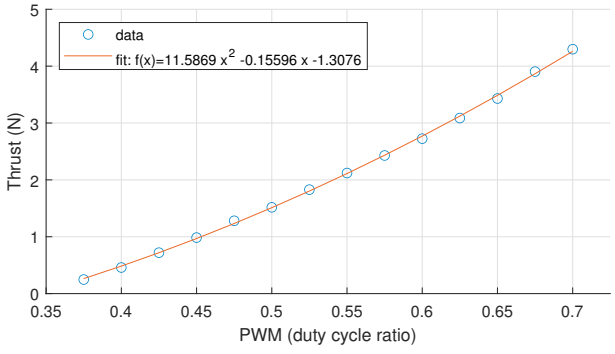

Fig. 2. Mapping between input and output

The thrust is not directly transmitted to the force sensor but through the support structure. The non-collocated nature of the inputs and outputs results in a non-minimum phase system for force transmission by the support structure (Figure 3). Thus, the structure imposes limitations on the frequency range of the signals that can be transmitted unaltered. From frequency response of the structure (Figure 3) the maximum frequency of the signal that is transmitted without attenuation is close to $314\,rad/s(\approx 50\,Hz)$ which is found to be sufficiently high for capturing the low frequency dynamics of the motor-propeller system.

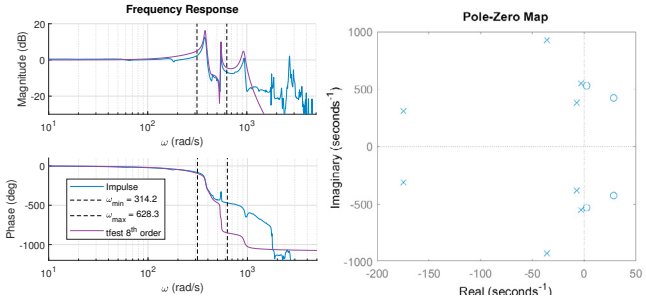

Fig. 3. Frequency response and pole-zero map of the estimated 8^{th} order transfer function of the structure

3. SYSTEM IDENTIFICATION

Input signal in PWM for system identification is generated using MyRio programmed in LabView. The force sensor data is acquired using a LabView VI and input-output synchronization is achieved through network shared variables whose latency is accounted for.

3.1 Input Generation

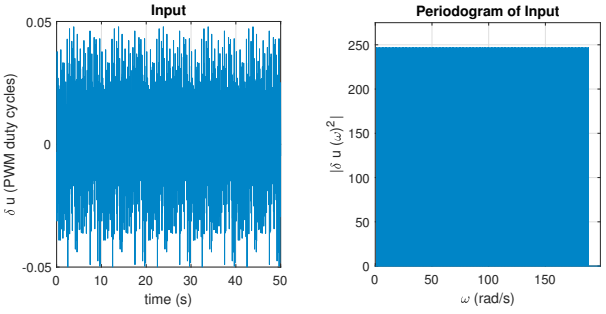

Fig. 4. Input for system identification.

A sum-of-sinusoids input using MATLAB's System Identification Toolbox (Ljung (2022)) with 150 frequencies in the frequency range $[0.1\,Hz\,(0.63\,rad/s), 30\,Hz\,(188.49\,rad/s)]$ (Figure 4) is used for system identification. The square wave response of the system is used for validation. The input signal is transformed in to the PWM signal around a nominal value (u_{nom}) and maximum perturbation ($\delta u = 0.05$), i.e., $u_{PWM} = \delta u \times u + u_{nom}$. The system identification is done at nominal inputs ranging from 0.4 to 0.7 at steps of 0.05 in PWM duty cycles.

3.2 Identification

The empirical transfer function estimates (ETFEs) calculated from the input-output data at given nominal inputs are shown in Figure 5. The frequency domain data is smoothened using Hann window (Ljung et al. (1987)). Based on empirical transfer function estimates, a first order model structure was found to sufficiently capture the dynamics in the chosen frequency range. Hence, we have the system model structure at given nominal input:

$$G_s(S) = \frac{K_s}{\tau_s s + 1} \tag{1}$$

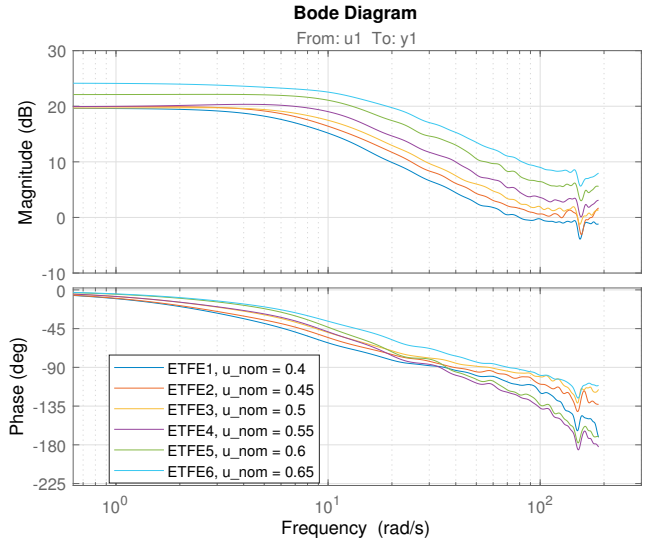

Fig. 5. Empirical Transfer Function Estimates (ETFEs) for a set of nominal inputs.

The ETFEs demonstrate the variation in the gain and time-constant of the model with change in the nominal input. The model parameters of the estimated first order transfer function including gain (K_s), time constant (τ_s) and cut-off frequency ($\omega_s = \frac{1}{\tau_s}$) are tabulated bellow in Table 1.

Table 1. Model parameters

u_{nom}	K_s	τ_s (s)	ω_s (rad/s)
0.4	9.9955	0.1593	6.2758
0.45	10.4556	0.1360	7.3524
0.5	10.1718	0.1077	9.2889
0.55	10.9196	0.1009	9.9130
0.6	13.4519	0.0852	11.7439
0.65	16.1063	0.0708	14.1275

3.3 Model Validation

The identified models are validated by comparing the simulated and actual response to a square wave input of amplitude 0.05 PWM duty cycles and an half-period of 5 s. The results of comparison, % fit (Ljung (2022)), are tabulated in Table 2.

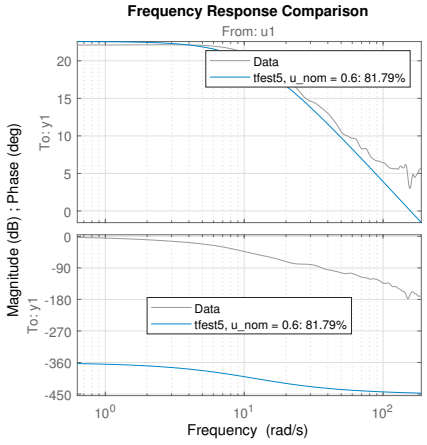

Fig. 6. Frequency domain model validation results

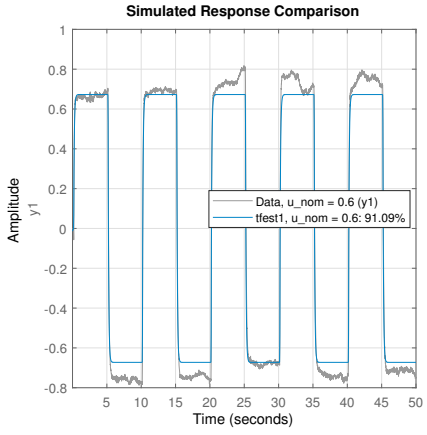

Fig. 7. Time domain validation results

Table 2. Model validation results

u_{nom}	Frequency Domain (%fit)	Square Wave Input (%fit)
0.4	89.9012	90.6762
0.45	89.0841	90.9004
0.5	89.3366	89.6856
0.55	79.3643	88.3727
0.6	81.7859	91.0912
0.65	91.5734	95.0363

The validation results show that the dynamic response of the system is captured by the model within reasonable error margins. The error in the static gain from the square-wave response is due to high variance in estimation of static gain from frequency response data (Ljung et al. (1987)).

4. OPEN-LOOP COMPENSATION

The response of the motor-propeller system can be sped-up by increasing the bandwidth of the system through open-loop compensation (Figure 8). The goal is to design one compensator across the input range of the actuator. Using the identified first order models, an open-loop compensator can be designed, which in the ideal case cancels the 'slower pole' at ω_s using its zero at $\omega_z (= \omega_s, \textit{ideally})$ and replaces it with a 'faster pole' at ω_f. The compensator increases the gain of the control-input for all the frequencies above

ω_s. This results in amplification of high-frequency input noise, which may be undesirable. Thus, the amplified frequency range is limited by introducing complex poles at ω_f, resulting in a second order system.

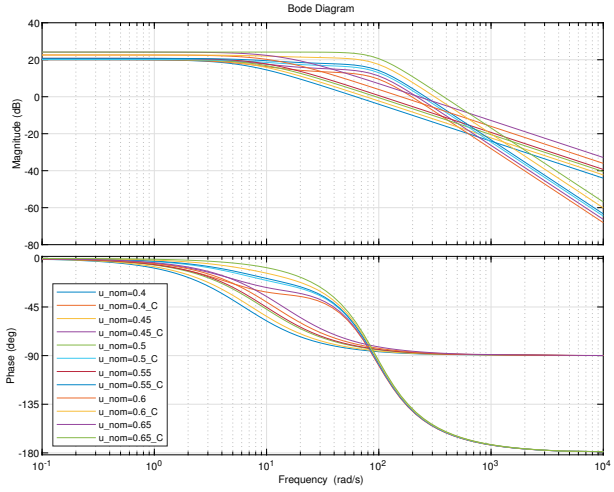

Fig. 8. Simulated frequency response of the system with and without open-loop compensation

4.1 Compensator Design

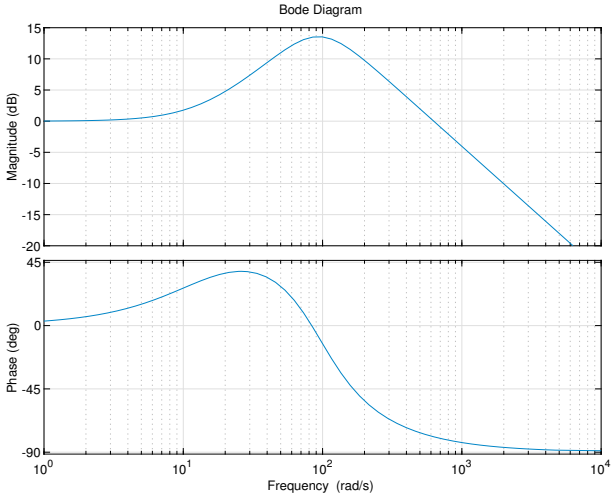

Fig. 9. Frequency response of the compensator

For such a second order system, the input is amplified only in the range $[\omega_s, \omega_g]$, where ω_g is the gain crossover frequency. The variation of system parameters with nominal inputs results in no pole-zero cancellation. This results in either a drop or raise in the gain of the compensated system between the frequencies corresponding to system's pole (at ω_s) and the compensator's zero (at ω_z). When, $\omega_z < \omega_s$, the system gain is amplified between ω_z and ω_s beyond the static gain of the system, which may cause instabilities and unnecessary overshoots in the response of the actuator. Thus,

$$\omega_z = \max\{\omega_s\} = 14.1275\ rad/s \tag{2}$$

The choice of ω_z imposes a lower limit on the cutoff-frequency of systems whose bandwidth can be increased by open loop compensation. Let this frequency be $\omega_{s_{min}}$. This is the cut-off frequency of the system whose bandwidth is less than ω_z rad/s. Using the frequency asymptotes in bode plots, $\omega_{s_{min}}$ can be calculated as follows:

$$\frac{0 - 3\ dB}{\log(\omega_z) - \log(\omega_{s_{min}})} = -20\ dB/dec$$
$$\implies \omega_{s_{min}} = \frac{\omega_z}{10^{3/20}} = 10.0015\ rad/s$$

Consequently, the proposed compensator will not significantly increase the bandwidth are lower nominal inputs (practically, $u_{nom} = 0.4$ and 0.45) as the cutoff frequencies of the linearized systems at those inputs are significantly lower than $\omega_{s_{min}}$ (Table 1). Practically, the multi-rotor vehicle's design ensures that the nominal input for hover conditions will be close to the middle of the overall input range. Hence, increasing the bandwidth at higher inputs will prove to be more useful. The resulting compensator will be of the form:

$$C(s) = \frac{\omega_f^2(\tau_z s + 1)}{s^2 + 2s\omega_f\zeta_f + \omega_f^2} \qquad where, \quad \tau_z = \frac{1}{\omega_z} \tag{3}$$

The input and output of the compensator are both PWM duty cycle (ratio). The static gain of the compensator is set to 1 so that the static response of the actuator remains unaltered. The parameters in the denominator of the compensator determine the overshoot in the actuator output due to compensation and the highest frequency at which the actuator output is amplified (ω_g). To avoid overshoot in compensated input,

$$\zeta_f = \frac{1}{\sqrt{2}} = 0.707 \tag{4}$$

Let, $\eta_f\ dB$ be the maximum gain, then

$$\frac{\eta_f - 0}{\log\omega_f - \log\omega_z} = 20, \qquad and \qquad \frac{0 - \eta_f}{\log\omega_g - \log\omega_f} = 20$$

$$\implies \omega_f = \sqrt{\omega_z\omega_g}, \qquad and \quad \eta_f = 10\log\frac{\omega_g}{\omega_z} \tag{5}$$

Assuming small signals and no input noise for present system, the maximum frequency that is amplified (ω_g), can be chosen to be equal to the sampling rate of the multi-rotor ($100Hz$).

$$\omega_g = (2\pi \times 100) = 628.32\ rad/s \quad \text{and} \tag{6}$$
$$\omega_z = \max\{\omega_s\} = 14.1275\ rad/s \tag{7}$$

we have,

$$\omega_f = 94.2157\ rad/s \quad \text{and} \tag{8}$$
$$\eta_f = 16.6811\ dB \tag{9}$$

Thus, substituting in (3), we have the open-loop compensator (10) for enhancing the bandwidth of the system. The frequency response of the compensator is shown in Figure 9.

$$C(s) = \frac{628.46s + 8876.60}{s^2 + 66.62s + 8876.60} \tag{10}$$

4.2 Validation

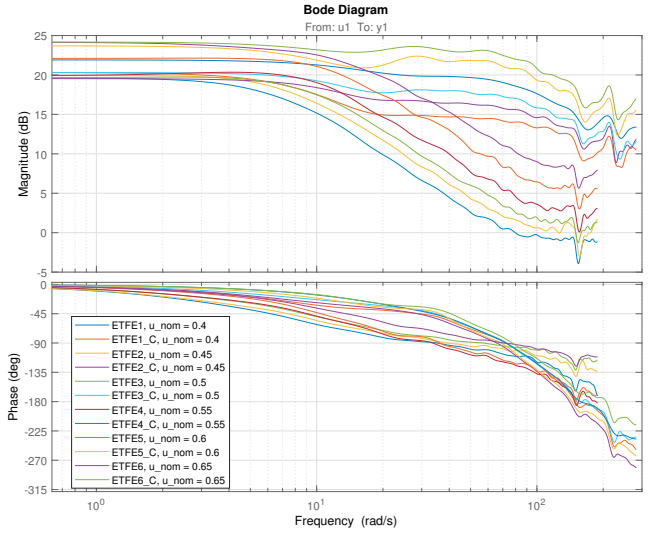

Fig. 10. Frequency Response of compensated and uncompensated systems

For validating the increase in bandwidth, the ETFEs of compensated system are estimated using a sum-of-sinusoids input in the range $[0.1\,Hz\,(0.63\,rad/s),\ 45\,Hz\,(282.74\,rad/s)]$. The increase in bandwidth can be clearly noted in comparison to the uncompensated system (Figure 10). The bandwidth of the compensated and uncompensated systems both from simulation and experiments is tabulated in Table 3.

Table 3. Bandwidth of the compensated and uncompensated system

u_{nom}	Bandwidth (rad/s)			
	uncompensated		compensated	
	Simulated	Experimental	Simulated	Experimental
0.4	6.2609	7.6139	8.0404	10.5564
0.45	7.3349	9.0941	10.8166	33.5233
0.5	9.2668	11.7689	24.5323	68.9652
0.55	9.8895	14.4992	41.4026	72.9550
0.6	11.7161	15.1641	74.6290	85.8608
0.65	14.0940	14.7953	94.1039	97.1847

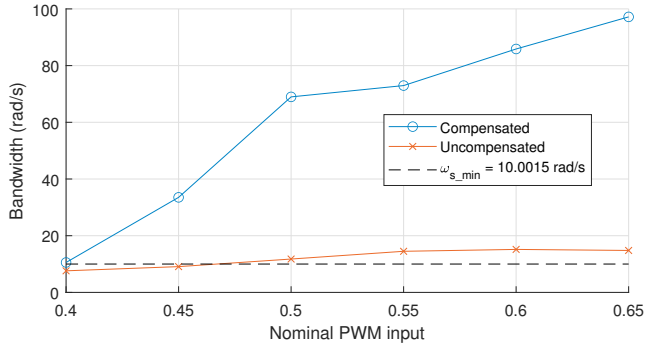

Fig. 11. Bandwidth of compensated and uncompensated systems at given nominal inputs

The frequency response of the compensated and uncompensated systems from the experiments match the simulation. As discussed previously, the bandwidth increase was not found to be significant in cases where the cutoff frequencies (ω_s) of the linearized system about the nominal inputs is less than $\omega_{s_{min}}$ (Figure 11). Thus, the open-loop compensator design is effective in enhancing the actuator bandwidth at the higher range of inputs.

Finally, the experimental results are compared with the simulation at the given set of nominal inputs in Figure 12 which shows consistent performance in the frequency range of interest.

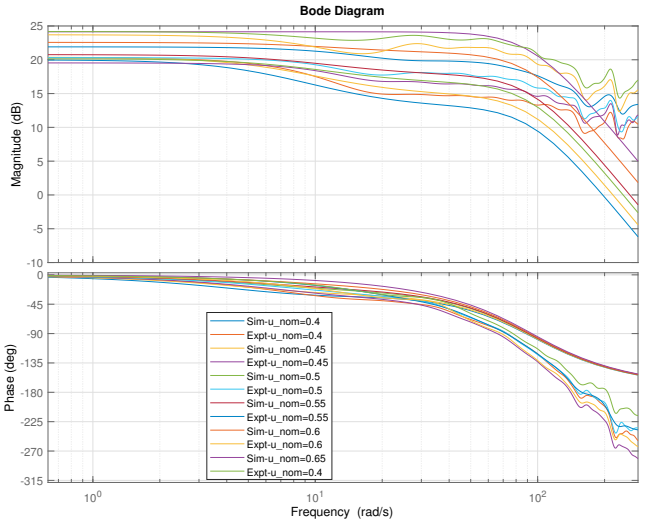

Fig. 12. Comparison between simulation and experimental frequency response of the compensated system

5. CONCLUSION

An open-loop compensator that increases the bandwidth of the actuator across higher range of the nominal inputs has been designed using the identified dynamics. On the actual drone, this just adds a compensator in the control algorithm and no additional hardware. System identification is done using small signals around the nominal inputs and the estimated models are validated. The effectiveness of the compensator on the motor-propeller system is demonstrated through non-parametric identification of the compensated system. The frequency response is found to be in agreement with the simulations validating the design methodology. The bandwidth increase is due to the zero of the compensator nullifying the effects of the pole of the actuator. This effect depends on the proximity of the zero to the pole and such a design would not prove effective if the parameters of the system vary drastically based on the input. The compensator design neglects the effects of higher order dynamics as they are not in the frequency range of interest. The effect of the compensator on higher frequency dynamics of the system has to be studied. This requires expanding the frequency range considered for system identification. For such analysis, the experimental setup has to be modified to increase the maximum frequency of the force that can be transmitted unaltered through the structure. This can be done either by increasing the stiffness of the structure or redesigning the system to have collocated inputs and outputs while still avoiding ground effects on the propeller thrust.

Further investigation on the effectiveness of such a compensator on the closed-loop bandwidth of the multi-rotor vehicle is needed. Such an analysis would lead to interesting insights into actuator performance in relation to the overall dynamics of the multi-rotor vehicle.

ACKNOWLEDGEMENTS

Prof. Voyles acknowledges the support of the NSF and the Center for Robots and Sensors for the Human Well Being (RoSe-HuB), under grant 1439717.

REFERENCES

Ding, C., Lu, L., Wang, C., and Ding, C. (2021). Design, sensing, and control of a novel uav platform for aerial drilling and screwing. *IEEE Robotics and Automation Letters*, 6(2), 3176–3183.

Franchi, A. and Mallet, A. (2017). Adaptive closed-loop speed control of bldc motors with applications to multi-rotor aerial vehicles. In *2017 IEEE International Conference on Robotics and Automation (ICRA)*, 5203–5208. IEEE.

Hamandi, M., Usai, F., Sablé, Q., Staub, N., Tognon, M., and Franchi, A. (2021). Design of multirotor aerial vehicles: A taxonomy based on input allocation. *The International Journal of Robotics Research*, 40(8-9), 1015–1044.

Jiang, G., Voyles, R., Sebesta, K., and Greiner, H. (2017). Estimation and optimization of fully-actuated multirotor platform with nonparallel actuation mechanism. In *2017 IEEE/RSJ International Conference on Intelligent Robots and Systems (IROS)*, 6843–6848. IEEE.

Liang, W., Chen, Z., and Yao, B. (2021). Geometric adaptive robust hierarchical control for quadrotors with aerodynamic damping and complete inertia compensation. *IEEE Transactions on Industrial Electronics*.

Ljung, L. (2022). *System identification toolbox: User's guide*. The MathWorks, Inc.

Ljung, L. et al. (1987). Theory for the user. *System Identification*.

Pounds, P., Mahony, R., and Corke, P. (2010). Modelling and control of a large quadrotor robot. *Control Engineering Practice*, 18(7), 691–699.

Pounds, P.E., Mahony, R.E., and Corke, P.I. (2009). Design of a static thruster for microair vehicle rotorcraft. *Journal of Aerospace Engineering*, 22(1), 85–94.

Ryll, M., Muscio, G., Pierri, F., Cataldi, E., Antonelli, G., Caccavale, F., and Franchi, A. (2017). 6d physical interaction with a fully actuated aerial robot. In *2017 IEEE International Conference on Robotics and Automation (ICRA)*, 5190–5195. IEEE.

Skogestad, S. and Postlethwaite, I. (2007). *Multivariable feedback control: analysis and design, Definition 2.1*, volume 2. Citeseer.

Tayebi, A. and McGilvray, S. (2006). Attitude stabilization of a vtol quadrotor aircraft. *IEEE Transactions on control systems technology*, 14(3), 562–571.

Townsend, W.T. and Salisbury, J.K. (1989). Mechanical bandwidth as a guideline to high-performance manipulator design. In *1989 IEEE International Conference on Robotics and Automation*, 1390–1391. IEEE Computer Society.

Wang, N., Su, S.F., Han, M., and Chen, W.H. (2018). Backpropagating constraints-based trajectory tracking control of a quadrotor with constrained actuator dynamics and complex unknowns. *IEEE Transactions on Systems, Man, and Cybernetics: Systems*, 49(7), 1322–1337.

Yacef, F., Bouhali, O., Hamerlain, M., and Rizoug, N. (2016). Observer-based adaptive fuzzy backstepping tracking control of quadrotor unmanned aerial vehicle powered by li-ion battery. *Journal of Intelligent & Robotic Systems*, 84(1), 179–197.